Generation and bistability of a waveguide nano-plasma observed by enhanced extreme ultraviolet fluorescence

Murat Sivis and Claus Ropers*
Institute of Materials Physics and Courant Research Center Nano-Spectroscopy and X-Ray Imaging, University of Göttingen, 37077 Göttingen, Germany

We present a study of the highly nonlinear optical excitation of noble gases in tapered hollow waveguides using few-femtosecond laser pulses. The local plasmonic field-enhancement induces the generation of a nanometric plasma, resulting in incoherent extreme ultraviolet fluorescence from optical transitions of neutral and ionized xenon, argon and neon. Despite sufficient intensity in the waveguide, high harmonic generation is not observed. The fluorescent emission exhibits a strong bistability manifest as an intensity hysteresis, giving strong indications for multistep collisional excitations.

PACS numbers: 52.50.Jm, 52.25.Os, 42.65.Pc, 73.20.Mf

arXiv:1304.0034v1 [physics.optics] 29 Mar 2013

Recent years have shown significant progress in translating concepts from strong-field atomic physics into the areas of ultrafast nano-optics and plasmonics. Numerous characteristic nonlinear optical phenomena, such as above-threshold and strong-field photoemission, have become accessible using local field enhancements in metal nanotips [1–5], resonant optical antennas [6–9], nanoparticles [10], rough surfaces [11] and plasmonic waveguides [12, 13]. These experimental studies are paralleled by increasing theoretical efforts of describing strong-field effects at surfaces and in optical near-fields [14–16], with a particular emphasis on nanostructure-enhanced high harmonic generation (HHG) [17–25]. Currently, some debate exists about experimental reports of nanostructure-enhanced HHG [6, 12, 13], following the demonstration of the predominance of incoherent extreme ultraviolet (EUV) fluorescence caused by multiphoton and strong-field atomic excitation and ionization [7, 9]. The essential physical issue revolves around the tendency of gaseous media in nanoscopic generation volumes to favor incoherent over coherent processes. Thus, although not all expectations on realizing novel forms of attosecond spectroscopy in compact devices may ultimately materialize experimentally, the discussion re-opens the field and further highlights the specificities and alternative scalings exhibited by strong-field interactions in nanostructures. This will allow for entirely new perspectives and phenomena in near-field high-intensity atomic and molecular gas excitations.

In this Letter, we demonstrate the nanostructure-enhanced formation of a confined plasma within a gas-filled plasmonic waveguide using low-energy, few-femtosecond laser pulses. This nano-plasma exhibits a pronounced threshold behavior and bistability of the fluorescent EUV emission that depends on the gas species and pressure. Specifically, we investigate the optical excitation, ionization and emission characteristics of xenon, argon and neon atoms and ions, and find strong indications that multistep collisional excitations contribute to an intensity hysteresis. Moreover, the exclusive observation of fluorescent emission highlights physical limits of nanostructure-based HHG concepts. Our results illustrate the plasmonic enhancement of strong-field effects in gaseous media and provide insight into the mechanisms associated with such phenomena driven at high repetition

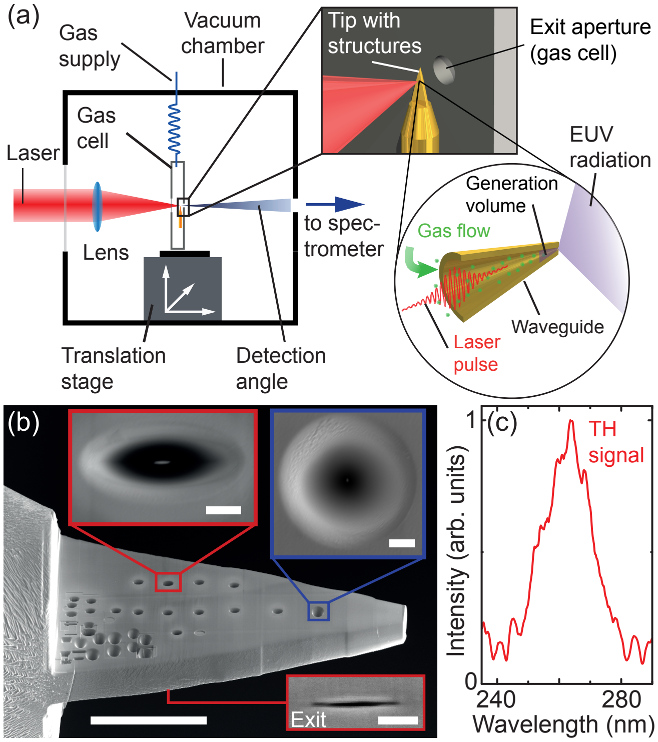

FIG. 1: (a) Schematics of the experimental setup. The generated radiation in a solid angle of ±1.2° is spectrally analyzed with a flat-field EUV spectrometer. (b) Scanning electron micrograph of the gold platform containing the tapered waveguides. Upper insets: close-up views of the entrance apertures of an elliptical and a circular waveguide. Lower inset: exit aperture of the elliptical waveguide. (Scale bars: overview 50 μm, top views 1 μm, exit aperture 200 nm). (c) Third harmonic signal generated in a waveguide without gas exposure.

rates and in nanoscale confinement.

The setup of our experiment is depicted in Fig. 1(a). An electrochemically etched gold tip containing the waveguide structures (cf. Fig. 1(b)) is placed in a cell that can be purged with different gases. The structures are mounted on micro translation stages (three translational and one rotational positioner) in a high vacuum chamber. Optical excitation with variable linear polarization is provided by 8-fs-pulses (800 nm center wavelength) from a 78 MHz titanium:sapphire laser oscillator, focused to a 5 μm spot size (FWHM). Incident peak-intensities up to about 1 TW/cm^2 are achieved. A 200 μm aperture in the gas cell allows for differential pumping of the detection chamber and the collection of the generated radiation. Spectral analysis is carried out with a home-built EUV flat-field spectrometer and a phosphor screen micro-channel-plate detector. A more detailed description of the detection scheme is given elsewhere [7, 9].

Various waveguides with circular and elliptical cross-sections are prepared on a 10 μm thick gold platform using focused ion beam etching (cf. Fig. 1(b)), and we have taken special care to produce smooth waveguide surfaces for minimal losses. For waveguides with elliptical entrance and exit apertures, geometrical dimensions are chosen that approximately correspond to those presented in Ref. [12], in which simulations indicated intensity enhancements of up to 350 near the waveguide end. As an example, Fig. 1(b) (inset, red frame) shows a waveguide with diameters of the minor and major axes of the entrance/exit apertures of 2.4 μm/40 nm and 4.8 μm/440 nm, respectively. Previously, optical second harmonic generation was used to characterize local fields at the exit aperture [26] of hollow near-field probes [27]. Here, we utilize surface-enhanced third harmonic (TH) generation as a confirmation of field enhancement and efficient waveguide coupling [9, 28–31]. Figure 1(c) displays a TH spectrum obtained from an illuminated waveguide in the absence of gas. To ensure a proper alignment and detection of any possible coherent contribution in the EUV radiation, the TH signal was optimized by adjusting the lateral positioning of the structures and the angle of incidence.

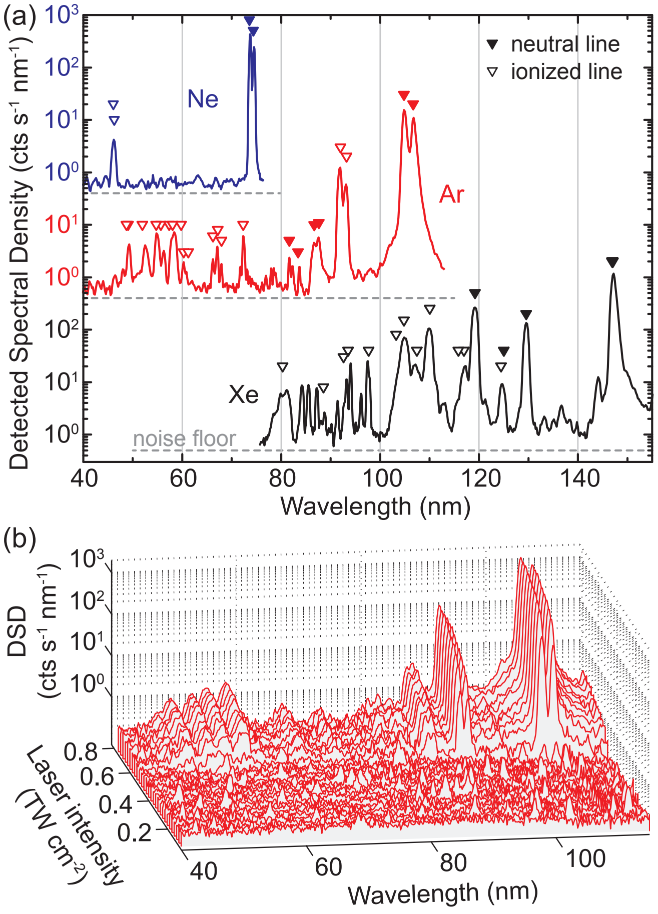

FIG. 2: (a) Nanostructure-enhanced EUV spectra (logarithmic scale) using xenon, argon and neon gas (200 mbar backing pressure) excited in the waveguide displayed in Fig.1(b) (inset, red frame). The argon and neon spectra are up-shifted for better visibility. In all cases, dashed gray lines correspond to the same signal level (being the noise floor at 0.5 cts/s/nm in these measurements). Wavelength positions of triangles indicate the expected fluorescent transitions for neutral (filled) and singly ionized (open) atoms of the respective gas species [32]. Providing for better resolution, the following portions of the spectra were recorded in the second grating diffraction order: Ne (>60 nm), Ar (65-84 nm), Xe (84-100 nm). (b) Intensity-dependent series of argon spectra recorded for increasing incident laser power.

In the following, we present our observations of the EUV radiation emitted from the illuminated structures exposed to atomic gases. Figure 2(a) shows EUV spectra measured using xenon (Xe), argon (Ar) and neon (Ne) gas in the elliptical waveguide displayed in Fig. 1(b) (inset, red frame). The spectra exhibit numerous emission lines at the atomic and ionic transitions of the respective elements (indicated by triangles [32]) and thus present incoherent characteristic EUV fluorescence, in other words atomic line emission (ALE). One of the essential features of the hollow waveguide structures, which has not yet been experimentally studied, is the theoretically proposed improvement in field-enhancement of an elliptical over a circular cross-section [12] and potential polarization dependencies. We have observed only minor EUV signals from waveguides with circular cross-sections, such as the one displayed in Fig. 1(b) (inset, blue frame). Moreover, we have studied the dependence of the EUV emission on incident laser polarization (cf. polar diagram in Fig. 3(a)). Maximum EUV intensity was found for a polarization parallel to the minor waveguide axis (corresponding to an angle of 0°), which is consistent with an interpretation that the fundamental excitation for polarization parallel to the minor axis reaches deeper into the waveguide and thus creates higher overall field enhancement.

Despite numerous tests, accurate alignments (cf. Fig 3(b)) and recording more than 2000 individual EUV spectra using different waveguides, intensities, gases and pressures, we have not found any indications for high harmonic generation in this spectral range, which appears to contradict the conclusions of previous reports [12, 13]. We note that the absence of HHG is not caused by insufficient local intensities, as is evident by the strong contributions from ionic transitions in our measured spectra. Substantial ionization is found even in neon with an ionization energy of 21.5 eV, exceeding the energy of 13 laser photons. The observations of a predominance of incoherent emission are consistent with our previous studies on plasmonic bow-tie antennas, in which sufficient near-field strengths generally allowing for HHG were verified by utilizing the intensity-dependent ALE spectral fingerprint [9]. Considering the field-enhanced volumes in both types of structures, severe limitations on high harmonic signal generation arise from the nanometric confinement of the source and the resulting insufficient coherent radiation build-up. Estimates on the relevant scalings are discussed in Refs. [9, 33].

It seems clear that these findings present a serious setback for current approaches to realize compact nanoscale sources of high harmonic radiation for attosecond spectroscopy. Nonetheless, it is apparent that the strong-field regime is reached by means of field-enhancement in these nanostructures. The long-term stability and reproducibility of the highly nonlinear EUV emission allows for further discovery in detailed investigations of the waveguide excitation and radiation mechanisms under such conditions.

To this end, we have carried out an analysis of the intensity- and pressure-dependencies of the emission for different gases. First, we find that as function of incident intensity–particularly for higher pressures–the fluorescent intensity exhibits a steep threshold behavior (displayed in Fig. 2(b)). This indicates a density-dependent plasma formation in the waveguide that is triggered by cascaded (for example collisional) excitation and ionization processes involving multiple excited atoms, ions or electrons. Moreover, at higher pressures, we find a pronounced and reproducible intensity hysteresis, i.e., a situation in which the fluorescent signal at a given incident intensity depends on the excitation history of the system. Figures 4(a), (b) display these intensity hysteresis curves for two different waveguide structures. Specifically, after having applied high intensity, substantial fluorescence can be maintained (upper branch) upon significantly decreasing the intensity to levels, at which hardly any fluorescence is detected when measured in conditions starting from low intensities (lower branch). In atomic gases, bistable behavior is a characteristic feature of complex plasma dynamics, which can manifest itself as hysteresis in the plasma properties upon cycling various physical parameters. The familiar effect of maintaining a gas-discharge for reduced voltages after ignition is just one example of such hystereses [34–37].

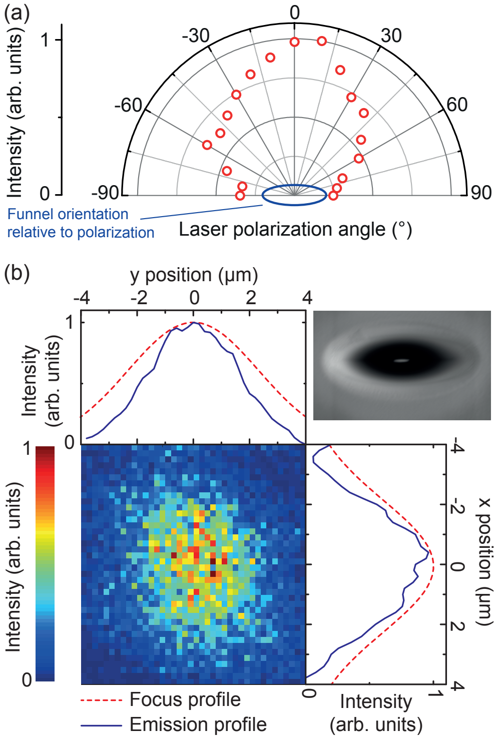

FIG. 3: (a) Intensity of the 104.8-nm argon line as a function of incident linear laser polarization. Polarization parallel to the minor axis leads to maximum fluorescent emission. (b) Emission map obtained for argon gas. The EUV fluorescence is recorded as the waveguide (cf. inset) is scanned relative to the focal spot. The averaged profiles in the x- and y-directions (solid blue) both show a significantly narrowed width compared with the focal laser profiles (dashed red), which is caused by spatial mode-overlap in conjunction with the emission nonlinearity.

The present observations constitute a new kind optical bistability [38] within metal nanostructures [39–41], which warrants further investigation. As expected for a bistable plasma effect, we find that it strongly depends on the gas species and pressure. In order to quantify the hysteresis, in Fig. 4(d), we evaluate the area enclosed by the two branches, normalized to the maximum fluorescent signal (Fig. 4(c)). The prominence of the bistability is found to increase more rapidly with increasing pressures for xenon compared with neon. Moreover, whereas it decreases beyond 150 mbar pressure in xenon, neon displays increasing hysteresis throughout the measured pressure range. The earlier onset of hysteresis for xenon is understood by considering that it has both a lower ionization threshold and a larger atomic cross-section for scattering events than neon. This results in reaching a critical excitation density for cascaded plasma formation at lower pressures.

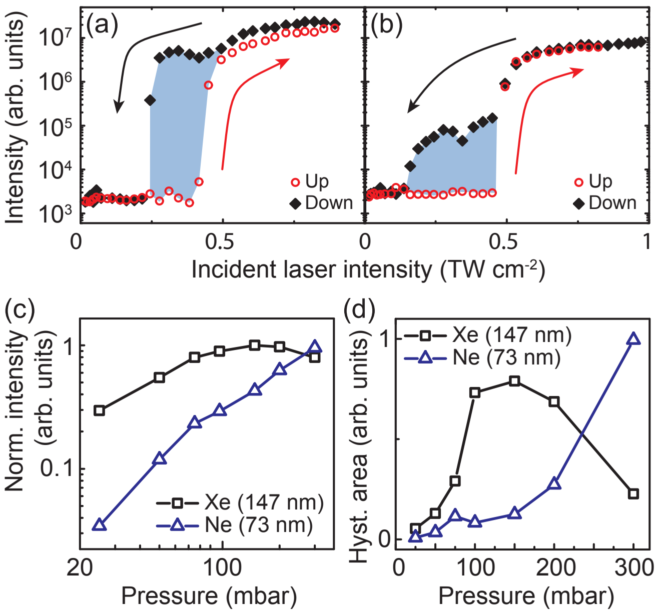

FIG. 4: (a),(b) Intensity-dependent strength of the 104.8-nm argon line excited in two different waveguides (pressure: 200 mbar). A pronounced intensity hysteresis is observed. (c) Pressure-dependent intensities of two prominent xenon and neon lines. (d) Degree of bistability in xenon and neon as a function of gas pressure, measured as the normalized area enclosed by the hysteresis curves (cf. shaded areas in (a) and (b)).

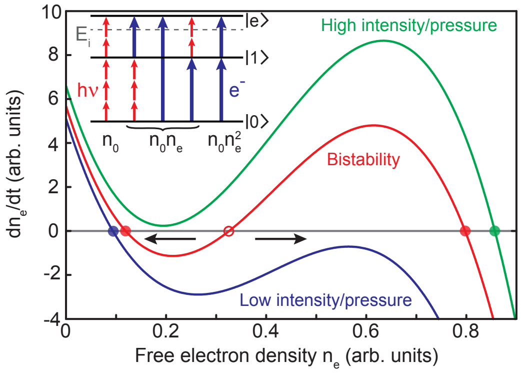

FIG. 5: Illustration of the appearance of bistability based on stepwise excitation processes. Ionization rate in the plasma as a function of free electron density for the laser intensities and/or gas pressures below (blue), within (red) and above (green) the bistable regime. Filled and open circles indicate stable and unstable zero-rate change conditions, respectively. Inset: Energy diagram with possible ionization paths via photon-driven (red arrows) and collisional (blue arrows) excitations.

A quantitative modeling of the plasma dynamics within the waveguide is outside of the scope of the present work, so that we give a qualitative description of the types of processes that will contribute to the observed bistability. Generally, the fact that a hysteresis is observed demonstrates that upon arrival of a laser pulse, there is residual excitation left within the waveguide from the previous excitation. After the laser pulse period of approximately 12 ns, the state of the system will be composed of partially decayed populations of excited states in neutral atoms and ions, free electrons, as well as thermal excitation of the gas and waveguide walls. As thermal transport in the bulk waveguide is rather efficient, the likely most relevant forms of residual excitation are long-lived atomic and ionic states. The reduced ionization energy of such states then causes a higher ionization rate than without prior excitation. An excitation memory alone, however, is not sufficient for the development of a bistability. Instead, the bistable behavior is caused by a collective aspect of the plasma dynamics, which influences the global state of the system and depends in a highly nonlinear way on the density of excited atoms or electrons.

The density of free electrons usually serves as the key marker for the state of a plasma, and it is instructive to discuss a stability diagram for the change of the degree of ionization on timescales much slower than the laser pulse period. Figure 5 qualitatively sketches the dependence of this (slow) rate of change of the electron density as a function of the density itself for conditions below (blue), within (red) and above (green) the bistable regime. Monostable conditions (green and blue) are necessarily characterized by a positive rate at zero density and negative rate at overly high density, with a single intersection at the stability point (zero rate change). A bistability implies two intersections and therefore requires at least a third-order power dependence of the electron production rate on the electron density.

The rate of change of the electron density is affected by numerous excitation and relaxation mechanisms, which in our case include multiphoton and strong-field ionization, together with collisional excitations from thermal or laser-field accelerated electrons, as well as collisional de-excitation and fluorescence. While such dynamics can be modeled in detail by coupled rate equations [35, 42], the density scaling of different excitation paths already provides adequate physical insight. The inset in Fig. 5 depicts several of the involved processes, together with the dependence of the electron production rate on the atom density in the ground state (n_0) and the free electron density (n_e). Both direct and stepwise processes via the numerous accessible atomic and ionic states (labeled by $|1\rangle$) contribute. Purely light-induced excitations and those involving up to one electron scattering event scale linearly and quadratically, respectively, in the densities. Stepwise ionization mechanisms involving two collisions (and possible further light-induced transitions not depicted) provide a third-order density scaling which may then cause bistable behavior. The explicit appearance of a rate contribution scaling as n_e^3 (as shown in Fig. 5) follows from elimination of n_0 by using the conservation of the overall mass density $\rho = n_0 + n_1 + n_e$.

Whereas other potential plasma effects could contribute to the observed bistability, the highly nonlinear pressure dependence of the hysteresis and the fact that accelerated electrons from strong-field photoionization with energies up to several tens of electronvoltsare present in significant density suggest that such multistep collisional excitations are a main mechanism inducing the bistability. Moreover, multiphoton and strong-field photoemisson from the waveguide walls [3, 4, 11] will provide additional electrons capable of collisional excitation. We have found that upon moderate waveguide modification by using incident powers in excess of 200 mW, the steepness of the threshold slope could be influenced, potentially by introducing roughness and thus altering the contributions from surface-emitted electrons.

In conclusion, we have demonstrated the formation of a sub-micron noble gas plasma within tapered waveguides by the observation of extreme ultraviolet fluorescence. Further studies will elucidate the different roles of surface-mediated, collisional and direct excitation processes. We believe that the possibility to induce highly nonlinear processes in these devices may lead to applications in the areas of EUV near-field imaging, lithography and spectroscopy. The observed bistability of the EUV emission strongly indicates cascaded excitation processes and presents a new link between nanostructure plasmonics and laser-induced surface plasma physics.

We thank M. Duwe, B. Abel, V. Radisch, B. Schröder and S. Schäfer for helpful discussions. Financial support by the Deutsche Forschungsgemeinschaft (DFG-ZUK 45/1 and SFB 755) is gratefully acknowledged.

---

* Electronic address: cropers@gwdg.de

[1] R. Bormann, M. Gulde, A. Weismann, S. V. Yalunin, and C. Ropers, Phys. Rev. Lett. **105**, 147601 (2010).

[2] M. Schenk, M. Krüger, and P. Hommelhoff, Phys. Rev. Lett. **105**, 257601 (2010).

[3] M. Krüger, M. Schenk, and P. Hommelhoff, Nature **475**, 78 (2011).

[4] G. Herink, D. R. Solli, M. Gulde, and C. Ropers, Nature **483**, 190 (2012).

[5] D. J. Park *et al.* Phys. Rev. Lett. **109**, 244803 (2012).

[6] S. Kim *et al.*, Nature **453**, 757 (2008).

[7] M. Sivis, M. Duwe, B. Abel, and C. Ropers, Nature **485**, E1 (2012).

[8] P. Dombi *et al.*, Nano Lett. **13**, 674 (2013).

[9] M. Sivis, M. Duwe, B. Abel, and C. Ropers, Nat. Phys. (2013, in press).

[10] S. Zherebtsov *et al.*, Nat. Phys. **7**, 656 (2011).

[11] P. Rácz, *et al.*, Appl. Phys. Lett. **98**, 111116 (2011).

[12] I.-Y. Park, *et al.*, Nat. Photon. **5**, 677 (2011).

[13] I.-Y. Park, *et al.*, Ann. Phys. **525**, 87 (2013).

[14] S. V. Yalunin, M. Gulde, and C. Ropers, Phys. Rev. B **84**, 195426 (2011).

[15] M. F. Ciappina *et al.*, Phys. Rev. A **86**, 023413 (2012).

[16] S. V. Yalunin *et al.*, Ann. Phys. **525**, L12 (2013).

[17] A. Husakou, S.-J. Im, and J. Herrmann, Phys. Rev. A **83**, 043839 (2011).

[18] A. Husakou, F. Kelkensberg, J. Herrmann, and M. J. J. Vrakking, Opt. Express **19**, 25346 (2011).

[19] S. L. Stabbings *et al.*, New J. Phys. **13**, 073010 (2011).

[20] T. Shaaran, M. F. Ciappina, and M. Lewenstein, Phys. Rev. A **86**, 023408 (2012).

[21] I. Yavus, E. A. Bleda, Z. Altun, and T. Topcu, Phys. Rev. A **85**, 013416 (2012).

[22] M. F. Ciappina, *et al.*, Opt. Express **20**, 26261 (2012).

[23] T. Shaaran, M. F. Ciappina, and M. Lewenstein, J. Mod. Opt. **59**, 1634 (2012).

[24] B. Fetić, K. Kalajdžić, and D. B. Milošević, Ann. Phys. **525**, 107 (2013).

[25] Y. Y. Yang *et al.*, Opt. Express **21**, 2195 (2013).

[26] M. Labardi *et al.*, Appl. Phys. Lett. **86**, 031105 (2005).

[27] C. Mihalcea *et al.*, Appl. Phys. Lett. **68**, 03531 (1996).

[28] T. Tsang, Phys. Rev. A **54**, 5454 (1996).

[29] M. Lippitz, M. A. van Dijk, and M. Orrit, Nano Lett. **5**, 799 (2005).

[30] T. Hanke *et al.*, Phys. Rev. Lett. **103**, 257404 (2009).

[31] M. Hentschel, T. Utikal, H. Giessen, and M. Lippitz, Nano Lett. **12**, 3778 (2012).

[32] J. E. Sansonetti, and W. C. Martin, J. Phys. Chem. Ref. Data **34**, 1559 (2005).

[33] M. Raschke, Ann. Phys. **525**, A40 (2013).

[34] U. Kortshagen, N. D. Gibson, and J. E. Lawlwe, J. Phys. D **29**, 1224 (1996).

[35] M. M. Turner and M. A. Lieberman, Plasma Sources Sci. Technol. **8**, 313 (1999).

[36] K. N. Ostrikov, S. Xu, and S. Lee, Phys. Scripta **62**, 189 (2000).

[37] Y. Chen, Z.-G. Guo, X.-M. Zhu, Z.-G. Mao, and Y.-K. Pu, J. Phys. D **40**, 5112 (2007).

[38] H. M. Gibbs, *Optical Bistability: Controlling Light with Light* (Academic, New York, 1985).

[39] G. Wurtz, R. Pollard, and A. Zayats, Phys. Rev. Lett. **97**, 057402 (2006).

[40] Y. Shen, and G. P. Wang, Opt. Express **16**, 8421 (2008).

[41] G. Wang, H. Lu, X. Liu, Y. Gong, and L. Wang, Appl. Opt. **50**, 5287 (2011).

[42] V. S. Vorob'ev and S. V. Maksimenko, Sov. J. Quantum Electron. **17**, 664 (1987).